Nonperturbative Shell-Model Interactions from the In-Medium Similarity Renormalization Group

S. K. Bogner, H. Hergert, J. D. Holt, A. Schwenk, S. Binder, A. Calci, J. Langhammer, and R. Roth

Phys. Rev. Lett. **113**, 142501 — Published 3 October 2014

DOI: 10.1103/PhysRevLett.113.142501

Nonperturbative shell-model interactions from the in-medium similarity renormalization group

S. K. Bogner,[1,*] H. Hergert,[2,†] J. D. Holt,[3,4,1,‡] A. Schwenk,[3,4,§]
S. Binder,[4] A. Calci,[4] J. Langhammer,[4] and R. Roth[4]

[1] *National Superconducting Cyclotron Laboratory and Department of Physics and Astronomy, Michigan State University, East Lansing, MI 48844, USA*
[2] *Department of Physics, The Ohio State University, Columbus, OH 43210, USA*
[3] *ExtreMe Matter Institute EMMI, GSI Helmholtzzentrum für Schwerionenforschung GmbH, 64291 Darmstadt, Germany*
[4] *Institut für Kernphysik, Technische Universität Darmstadt, 64289 Darmstadt, Germany*

We present the first *ab initio* construction of valence-space Hamiltonians for medium-mass nuclei based on chiral two- and three-nucleon interactions using the in-medium similarity renormalization group. When applied to the oxygen isotopes, we find experimental ground-state energies are well reproduced, including the flat trend beyond the drip line at ^{24}O. Similarly, natural-parity spectra in ^{21,22,23,24}O are in agreement with experiment, and we present predictions for excited states in ^{25,26}O. The results exhibit a weak dependence on the harmonic-oscillator (HO) basis parameter and reproduce spectroscopy within the standard *sd* valence space.

PACS numbers: 21.30.Fe, 21.60.Cs, 21.60.De, 21.10.-k

With the next generation of rare-isotope beam facilities, the quest to discover and understand the properties of exotic nuclei from first principles is a fundamental challenge for nuclear theory. This challenge is complicated in part because the proper inclusion of three-nucleon (3N) forces plays a decisive role in determining the structure of medium-mass nuclei [1, 2]. While *ab initio* many-body methods based on nuclear forces from chiral effective field theory (EFT) [3–5] have now reached the medium-mass region and beyond [6–20], restrictions in the nuclei and observables accessible to these methods have limited their application primarily to ground-state properties in semi-magic isotopic chains.

For open-shell systems, rather than solving the full A-body problem, it is profitable to follow the shell-model paradigm by constructing and diagonalizing an effective Hamiltonian in which the active degrees of freedom are A_v valence nucleons confined to a few orbitals near the Fermi level. Both phenomenological and microscopic implementations of the shell model have been used with success to understand and predict the evolution of shell structure, properties of ground and excited states, and electroweak transitions [21–23].

Recent microscopic shell-model studies have revealed the impact of 3N forces in predicting ground- and excited-state properties in neutron- and proton-rich nuclei [1, 2, 24–28]. Despite the novel insights gained from these studies, they make approximations which are difficult to benchmark. The microscopic derivation of the effective valence-space Hamiltonian relies on many-body perturbation theory (MBPT) [29], where order-by-order convergence is unclear. Even with efforts to calculate particular classes of diagrams nonperturbatively [30], results are sensitive to the HO frequency $\hbar\omega$ (due to the core), and the choice of valence space [2, 24, 25]. A nonperturbative method to address these issues was developed in [31, 32], which generates valence-space interactions and operators by projecting their full no-core shell model (NCSM) counterparts into a given valence space.

To overcome these limitations in heavier systems, the in-medium similarity renormalization group (IM-SRG), originally developed for *ab initio* calculations of ground states in closed-shell systems [33], can be extended to derive effective valence-space Hamiltonians and operators nonperturbatively. Calculations without initial 3N forces [34] indicated that an *ab initio* description of ground and excited states for open-shell nuclei may be possible with this approach. In this Letter, we apply the IM-SRG starting from chiral nucleon-nucleon (NN) and 3N forces to the more challenging and physically interesting problem of the oxygen isotopes.

The IM-SRG is a continuous unitary transformation $U(s)$, parameterized by a flow parameter s, that drives the Hamiltonian to a band- or block-diagonal form [35]. This is accomplished by solving the flow equation

$$\frac{dH(s)}{ds} = [\eta(s), H(s)]\,, \tag{1}$$

where $\eta(s) \equiv [dU(s)/ds]\,U^\dagger(s)$ is the anti-Hermitian generator of the transformation. With a suitable choice of $\eta(s)$, the off-diagonal part of the Hamiltonian, $H^{\rm od}(s)$, is driven to zero as s approaches ∞. The "in-medium" label indicates that we control the proliferation of induced many-body operators by normal ordering the Hamiltonian with respect to a finite-density reference state for each system of interest. We truncate Eq. (1) to normal-ordered two-body operators, which we refer to as the IM-SRG(2) approximation. Initial results for ^{6}Li agreed well with NCSM [34], and a quantitative comparison with the importance-truncated NCSM [36] is underway.

The utility of the IM-SRG lies in the freedom to tailor the definition of $H^{\rm od}$ to a specific problem. For instance,

to construct a shell-model Hamiltonian for a nucleus comprised of A_v valence nucleons outside a closed core, we define a Hartree-Fock (HF) reference state $|\Phi\rangle$ for the core with A_c particles, and split the single-particle basis into hole (h), valence (v), and non-valence (q) particle states. Treating all A nucleons as active, we eliminate matrix elements which couple $|\Phi\rangle$ to excitations, just as in IM-SRG ground-state calculations [13, 14, 33]. In addition, we decouple states with A_v particles in the valence space, $:a^\dagger_{v_1}\dots a^\dagger_{v_{A_v}}:|\Phi\rangle$, from states containing non-valence states.

Normal-ordering the Hamiltonian with respect to $|\Phi\rangle$ and working in the IM-SRG(2) truncation

$$H(s) = E_0 + \sum_{ij} f_{ij}\ :a^\dagger_i a_j: + \frac{1}{4}\sum_{ijkl}\Gamma_{ijkl}\ :a^\dagger_i a^\dagger_j a_l a_k:, \tag{2}$$

we define [34]

$$\left\{H^{\rm od}\right\} = \left\{f_{ph}, f_{pp'}, f_{hh'}, \Gamma_{pp'hh'}, \Gamma_{pp'vh}\,, \Gamma_{pqvv'}\right\} + \text{H.c.} \tag{3}$$

and use the White generator defined in Refs. [13, 33, 34]. With this choice of generator, $H^{\rm od}(\infty) \to 0$, and the shell-model Hamiltonian is obtained by taking all valence-space matrix elements.

We start from the chiral N^{3}LO NN interaction of Refs. [4, 37], with cutoff $\Lambda_{\rm NN} = 500$ MeV and apply a free-space SRG evolution to lower the momentum resolution scale, $\lambda_{\rm SRG}$. The NN+3N-induced Hamiltonian consistently includes three-nucleon forces induced by the evolution. Results for this interaction correspond to the unevolved NN interaction, up to truncated induced 4N,...,AN forces [38, 39]. The NN+3N-full Hamiltonians also include an initial local chiral 3N interaction at order N^{2}LO [40], consistently evolved to $\lambda_{\rm SRG}$. We consider two cutoffs for the initial 3N interaction, $\Lambda_{\rm 3N} = 400, 500$ MeV. The latter is naively consistent with $\Lambda_{\rm NN}$, although the NN interaction uses non-local regulators. Due to the reduced cutoff, the former avoids induced 4N interactions as $\lambda_{\rm SRG}$ is lowered [10, 41]. The Hamiltonian has 27 low-energy constants in the NN interaction plus two from the 3N interaction, which are fit to properties of few-body systems only, thereby providing predictions when applied to the medium-mass region.

The SRG-evolved Hamiltonians are transformed to an angular-momentum-coupled basis built from single-particle HO states with quantum numbers $e = 2n + l \leq e_{\rm max}$. An additional cut $e_1 + e_2 + e_3 \leq E_{\rm 3max} < 3e_{\rm max}$ is introduced to manage storage of the 3N matrix elements. We use $E_{\rm 3max} = 14$, which for resolution scales $\lambda_{\rm SRG} = 1.88 - 2.24$ fm^{-1} contributes less than 1% to the uncertainty of ground-state energies [10, 12–14, 18].

We first solve the HF equations for the ^{16}O core using the intrinsic kinetic energy,

$$T_{\rm int} = T - T_{\rm cm} = \left(1 - \frac{1}{A}\right)\sum_i \frac{\boldsymbol{p}_i^2}{2m} - \frac{1}{Am}\sum_{i<j}\boldsymbol{p}_i\cdot\boldsymbol{p}_j\,, \tag{4}$$

with A being the particle number of the *target nucleus* to account for the change of the single-particle wavefunctions as $A_c \to A$ [42]. The Hamiltonian is then normal ordered with respect to the core's HF reference state, and the resulting in-medium zero-, one-, and two-body operators serve as the initial values for the IM-SRG flow equations. The residual three-body term is neglected, giving rise to the normal-ordered two-body (NO2B) approximation [7, 10, 12]. The one- and two-body parts of the fully decoupled valence-space Hamiltonian are taken as the single-particle energies (SPEs) and two-body matrix elements to be diagonalized in a standard shell-model calculation, which we diagonalize in the *sd* valence-space above an inert ^{16}O core.

TABLE I. IM-SRG *sd*-shell SPEs (in MeV) for $\lambda_{\rm SRG} = 1.88\,\text{fm}^{-1}$ and $\hbar\omega = 24$ MeV, compared with MBPT [24] (NN+3N, see text) and phenomenological USDb values [43].

Orbit	NN	NN+3N-ind.	NN+3N-full		MBPT	USDb
			400 MeV	500 MeV		
$d_{5/2}$	−7.07	−3.77	−4.62	−7.14	−3.78	−3.93
$s_{1/2}$	−5.80	−2.46	−2.96	−4.42	−2.42	−3.21
$d_{3/2}$	1.81	2.33	3.17	2.85	1.45	2.11

Of interest is the $\hbar\omega$ dependence of the spectra, since $\hbar\omega$ is adjusted to the core in phenomenological shell-model calculations. We illustrate the effect of varying $\hbar\omega$ from 20 MeV to 24 MeV by shaded bands in all plots. Since this variation probes the convergence of the calculation and is mainly governed by $\lambda_{\rm SRG}$ rather than the input Hamiltonian, we only show bands for the NN+3N-full Hamiltonians. Finally, coupling to the continuum is relevant in neutron-rich oxygen isotopes [8, 44], and we will include these effects in future work. We indicate in all spectra the location of the neutron- separation threshold to highlight the energy region where continuum is expected to become important.

The IM-SRG SPEs are given in Table I. We compare to SPEs calculated in MBPT, from softened N^{3}LO NN and re-fit N^{2}LO 3N interactions [1, 2, 38], and from phenomenological USDb [43]. The NN case, where the IM-SRG SPEs are significantly overbound, requires induced 3N to improve the description. For NN+3N-full, the $\Lambda_{\rm 3N} = 400$ MeV SPEs are comparable to MBPT and phenomenology, while those from $\Lambda_{\rm 3N} = 500$ MeV are more deeply bound. The $d_{5/2} - d_{3/2}$ gap is approximately 2 MeV (4 MeV for $\Lambda_{\rm 3N} = 500$ MeV) larger in IM-SRG, pointing to a stronger spin-orbit component than in MBPT.

Because of the deeply bound SPEs for $\Lambda_{\rm 3N} = 500$ MeV, excited states lie $1.0 - 1.5$ MeV higher in energy than for $\Lambda_{\rm 3N} = 400$ MeV. This variation should be regarded only as a first step towards estimating the uncertainty, since it conflates uncertainties from the input Hamiltonian with those from the evolution to $\lambda_{\rm SRG}$. For $\Lambda_{\rm 3N} = 400$ MeV,

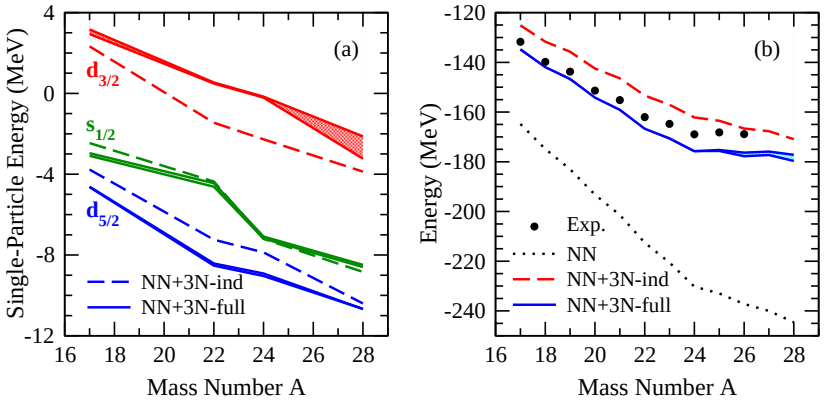

FIG. 1. Single-particle energy evolution (a) and ground-state energies (b) for A-dependent Hamiltonian with $\lambda_{\rm SRG} = 1.88\,{\rm fm}^{-1}$. The range of NN+3N-full ($\Lambda_{\rm 3N} = 400\,{\rm MeV}$) results for $\hbar\omega = 20, 24\,{\rm MeV}$ is given by the shaded bands.

these uncertainties are controlled, and we can directly confront the input chiral Hamiltonian with experiment [12–14, 18, 41]. For this reason, we only discuss the spectra for this Hamiltonian in detail in the following.

The importance of 3N forces in determining the oxygen dripline was first highlighted in microscopic valence-space calculations [1, 24, 45], then in *ab initio* studies [8, 14, 15]. The evolution of the IM-SRG SPEs with the neutron number (Fig. 1(a)) reveals the same mechanism: in the NN+3N-induced case, the $d_{3/2}$ orbit remains bound past ^{20}O. The repulsive effects of 3N forces shift the $d_{3/2}$ orbit to a higher starting point of 3.17 MeV in ^{17}O, while moderating its decrease to neutron-rich isotopes, where it is bound by only 160 keV in ^{24}O.

We diagonalize the A-dependent IM-SRG valence-space Hamiltonian to obtain the ground-state energies of $^{18-28}$O, shown in Fig. 1(b), which include the IM-SRG-calculated core energy. For an SRG-evolved NN interaction, the oxygen isotopes are overbound due to neglected initial and induced 3N forces, leading to unrealistic predictions. Including induced 3N forces lessens the overbinding, but fails to give the correct trend past ^{24}O. With initial 3N forces, agreement with experimental data is further improved, with moderate overbinding past ^{22}O. Moreover, the flat trend of the ground-state energies beyond ^{24}O is similar to experimental data in ^{25,26}O [45–47] and agrees with other calculations based on chiral NN+3N forces [1, 8, 15, 24]. We note that $^{25-28}$O are weakly bound w.r.t. ^{24}O. Finally, $\Lambda_{\rm 3N} = 500\,{\rm MeV}$ ground-state energies are overbound with more pronounced $\lambda_{\rm SRG}$ dependence. For instance in ^{22,24,28}O, energies increase, respectively, to $-202.18\,{\rm MeV}$, $-215.42\,{\rm MeV}$, $-219.94\,{\rm MeV}$ for $\lambda_{\rm SRG} = 1.88\,{\rm fm}^{-1}$ and $-193.31\,{\rm MeV}$, $-204.30\,{\rm MeV}$, $-206.85\,{\rm MeV}$ for $\lambda_{\rm SRG} = 2.24\,{\rm fm}^{-1}$.

In contrast, the multi-reference IM-SRG (MR-IM-SRG) [14] gives a robust prediction of the dripline at ^{24}O for the NN+3N-full Hamiltonians, with ground-state energies in good agreement with experimental data and

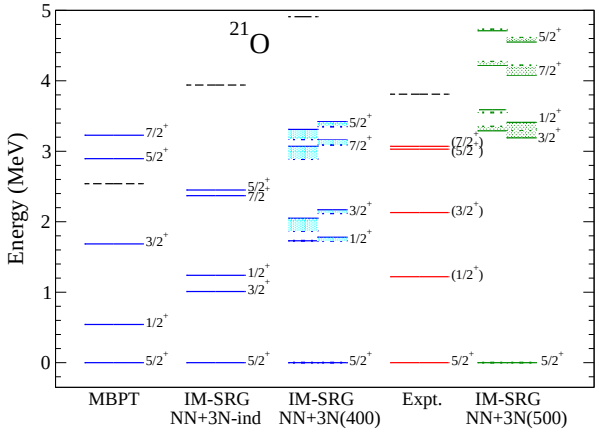

FIG. 2. Excited-state spectrum of ^{21}O for IM-SRG Hamiltonians based on NN+3N-induced and NN+3N-full for $\Lambda_{\rm 3N} = 400, 500\,{\rm MeV}$, with $\hbar\omega = 20\,{\rm MeV}$ (dotted) and $\hbar\omega = 24\,{\rm MeV}$ (solid), compared with MBPT (NN+3N) and experiment [48]. NN+3N-full results are given in two columns: $\lambda_{\rm SRG} = 1.88\,{\rm fm}^{-1}$ (left) and $\lambda_{\rm SRG} = 2.24\,{\rm fm}^{-1}$ (right). The neutron-separation threshold is given by black dot-dashed lines.

other *ab initio* methods [14]. The MR-IM-SRG evolution is carried out in the target nucleus rather than in the core with shifted A, so its open-shell reference state accounts for wavefunction-relaxation effects and the presence of nucleons in the valence space during the evolution. Therefore differences like the observed $< 2\%$ are to be expected. We will revisit the issue of over-binding by using ^{22}O and ^{24}O cores and compare these results with MR-IM-SRG calculations of excited states.

In Fig. 1(b), we highlight the insensitivity of the ground-state energies to variation of $\hbar\omega$ from 20 MeV to 24 MeV in the band for the NN+3N-full Hamiltonian. Differences only become non negligible for $A > 24$. The weak dependence of calculated observables on $\hbar\omega$ is a striking feature of the nonperturbative IM-SRG valence-space approach, implying a remarkable level of conver-

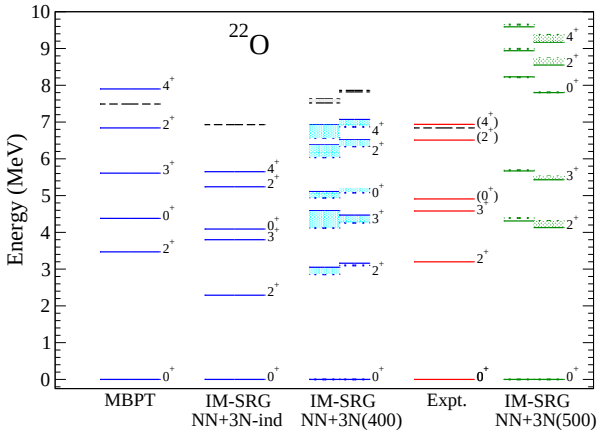

FIG. 3. Excited state spectrum for ^{22}O as in Fig. 2, with experimental values from [48, 49].

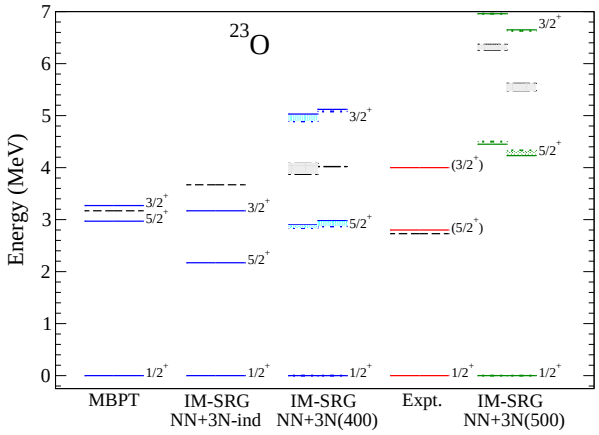

FIG. 4. Excited state spectrum of ^{23}O as in Fig. 2, with experimental values from [50, 51].

gence at the IM-SRG(2) level.

Turning to excitation spectra, since NN forces give a reasonable description of low-lying spectra near ^{16}O [29], we focus on the region of the new $N = 14, 16$ magic numbers, and the limit of stability by considering $^{21-26}$O. As shown in Ref. [24], microscopic valence-space Hamiltonians from MBPT, calculated in the standard *sd*-shell, do not adequately reproduce experimental data, even with 3N forces. With the inclusion of the $f_{7/2}$ and $p_{3/2}$ orbitals, spectroscopy improves, indicating that a perturbative treatment of these orbitals may be insufficient. Given the nonperturbative character of IM-SRG, we expect similar improvements already in the *sd* shell.

We first consider the spectrum of ^{21}O in Fig. 2. While no calculation fully reproduces experiment, MBPT and IM-SRG correctly predict the ordering of the first two excited states with an initial 3N force, but the $1/2^+$ level lies too low in MBPT and too high in IM-SRG. Since the MBPT results are obtained with a softened N^{3}LO interaction with a re-fit 3N interaction [1, 2], disagreements are both due to the different input Hamiltonians and the nonperturbative IM-SRG approach. We note that the tentative $7/2^+$ and $5/2^+$ assignments are reproduced in both calculations, but the ordering is reversed in IM-SRG compared to MBPT.

The calculated IM-SRG spectra of ^{22}O are compared with MBPT [24] and experiment [48, 49] in Fig. 3. Without initial 3N forces, the spectrum is too compressed. The 2_1^+ state, in particular, is 1.0 MeV too low, contradicting the doubly magic nature of ^{22}O. Unlike MBPT or the phenomenological USDb Hamiltonian, the IM-SRG reproduces the correct ordering of the 3_1^+ and 0_2^+ states. Inclusion of initial 3N forces leads to significant improvement, and the final spectrum is very close to experiment. The extended-space MBPT calculations reproduce the high 2_1^+ state but have too uniform spacing and incorrect $3_1^+ - 0_2^+$ ordering.

There are no bound excited states in ^{23}O, only two higher-lying states, tentatively identified as $5/2^+$ and $3/2^+$, indicating the sizes of the $d_{5/2}-s_{1/2}$ and $d_{3/2}-s_{1/2}$ gaps, respectively [50, 51]. We show the calculated and experimental spectra in Fig. 4. Again, the IM-SRG does not reproduce this spectrum without initial 3N forces: the $5/2^+$ state is nearly 1 MeV too low, but the $5/2^+ - 3/2^+$ gap close to experiment. Similar to MBPT with initial 3N forces, the $5/2^+$ energy is almost exactly that of experiment, only the $3/2^+$ is 1 MeV too high. Due to its position 2 MeV above threshold, it is expected that continuum effects will lower this state, bringing it closer to the experimental value.

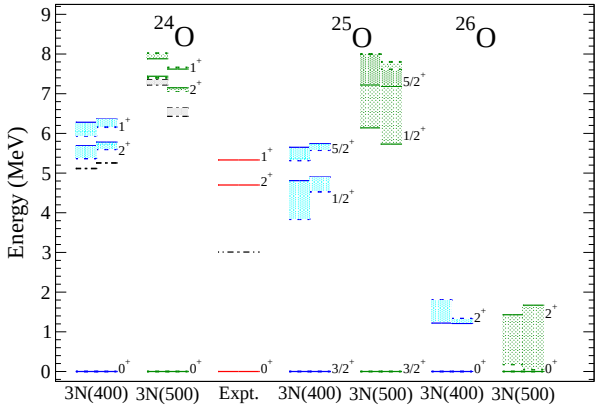

FIG. 5. Excited state spectra of $^{24-26}$O for $\Lambda_{3N} = 400, 500$ MeV NN+3N-full Hamiltonians with $\hbar\omega = 20$ MeV (dotted), $\hbar\omega = 24$ MeV (solid), and λ_{SRG} dependence as in Fig. 2, compared to experiment for ^{24}O [52, 53].

As expected from the high $3/2^+$ state in ^{23}O, we also predict ^{24}O to be doubly magic, but with a 2_1^+ energy 1.2 MeV higher than experiment, as seen in Fig. 5. Nonetheless, the $2^+ - 1^+$ spacing is very close to experiment, and with continuum effects included, these states will be lowered. Finally, we present predictions for excited-state energies in the unbound ^{25,26}O isotopes.

We again find large $1/2^+$ and $5/2^+$ excitation energies in ^{25}O, which are expected to decrease with continuum coupling. In ^{26}O, we predict one low-lying state below 6 MeV: a 2^+ near 2 MeV. A tentative identification of an excited state near 4 MeV was reported in [45], but no such natural-parity state was found in our calculations.

We have presented the first *ab initio* construction of a nonperturbative *sd*-shell Hamiltonian based on chiral NN and 3N forces. The SPEs and two-body matrix elements are well converged with respect to basis size and exhibit weak $\hbar\omega$ dependence. Furthermore, a good description of ground and excited states is found throughout the oxygen isotopes in a valence space consisting of only the *sd*-shell orbits. This provides the exciting possibility to extend these calculations to nearby F, Ne, and Mg isotopic chains and through extending the valence space, will give access to the island-of-inversion region and potentially the full *sd*-shell neutron dripline.

Acknowledgments. We thank R. Furnstahl, M. Hjorth-Jensen, C. R. Hoffman, and J. Menéndez for useful discussions. This work was supported in part by the NUCLEI SciDAC Collaboration under the U.S. Department of Energy Grants No. DE-SC0008533 and DE-SC0008511, the National Science Foundation under Grants No. PHY-1002478, PHY-1306250, and PHY-1068648, the Helmholtz Alliance Program of the Helmholtz Association, contract HA216/EMMI "Extremes of Density and Temperature: Cosmic Matter in the Laboratory", the DFG through grant SFB 634, the BMBF under Contract No. 06DA70471 the ERC (grant 307986 STRONGINT), and HIC for FAIR. Computing resources were provided by the Ohio Supercomputing Center (OSC).

* E-mail: bogner@nscl.msu.edu
† E-mail: hergert.3@osu.edu
‡ E-mail: jason.holt@physik.tu-darmstadt.de
§ E-mail: schwenk@physik.tu-darmstadt.de

[1] T. Otsuka, T. Suzuki, J. D. Holt, A. Schwenk, and Y. Akaishi, Phys. Rev. Lett. **105**, 032501 (2010).
[2] J. D. Holt, T. Otsuka, A. Schwenk, and T. Suzuki, J. Phys. G **39**, 085111 (2012).
[3] E. Epelbaum, H.-W. Hammer, and U.-G. Meißner, Rev. Mod. Phys. **81**, 1773 (2009).
[4] R. Machleidt and D. Entem, Phys. Rept. **503**, 1 (2011).
[5] H.-W. Hammer, A. Nogga, and A. Schwenk, Rev. Mod. Phys. **85**, 197 (2013).
[6] G. Hagen, T. Papenbrock, D. J. Dean, and M. Hjorth-Jensen, Phys. Rev. C **82**, 034330 (2010).
[7] G. Hagen, T. Papenbrock, D. J. Dean, A. Schwenk, A. Nogga, M. Włoch, and P. Piecuch, Phys. Rev. C **76**, 034302 (2007).
[8] G. Hagen, M. Hjorth-Jensen, G. R. Jansen, R. Machleidt, and T. Papenbrock, Phys. Rev. Lett. **108**, 242501 (2012).
[9] G. Hagen, M. Hjorth-Jensen, G. R. Jansen, R. Machleidt, and T. Papenbrock, Phys. Rev. Lett. **109**, 032502 (2012).
[10] R. Roth, S. Binder, K. Vobig, A. Calci, J. Langhammer, and P. Navrátil, Phys. Rev. Lett. **109**, 052501 (2012).
[11] V. Somá, C. Barbieri, and T. Duguet, Phys. Rev. C **87**, 011303 (2013).
[12] S. Binder, J. Langhammer, A. Calci, P. Navrátil, and R. Roth, Phys. Rev. C **87**, 021303 (2013).
[13] H. Hergert, S. K. Bogner, S. Binder, A. Calci, J. Langhammer, R. Roth, and A. Schwenk, Phys. Rev. C **87**, 034307 (2013).
[14] H. Hergert, S. Binder, A. Calci, J. Langhammer, and R. Roth, Phys. Rev. Lett. **110**, 242501 (2013).
[15] A. Cipollone, C. Barbieri, and P. Navrátil, Phys. Rev. Lett. **111**, 062501 (2013).
[16] G. R. Jansen, Phys. Rev. C **88**, 024305 (2013).
[17] V. Somá, A. Cipollone, C. Barbieri, P. Navrátil, and T. Duguet, Phys. Rev. C **89**, 061301(R) (2014).
[18] S. Binder, J. Langhammer, A. Calci, and R. Roth, Phys. Lett. B **736**, 119 (2014).
[19] G. Hagen, T. Papenbrock, M. Hjorth-Jensen, and D. Dean, (2013), arXiv:1312.7872 [nucl-th].
[20] T. A. Lähde, E. Epelbaum, H. Krebs, D. Lee, U.-G. Meißner, *et al.*, Phys. Lett. B **732**, 110 (2014).
[21] B. A. Brown, Prog. Part. Nucl. Phys. **47**, 517 (2001).
[22] E. Caurier, G. Martinez-Pinedo, F. Nowacki, A. Poves, and A. Zuker, Rev. Mod. Phys. **77**, 427 (2005).
[23] T. Otsuka, Physica Scripta **2013**, 014007 (2013).
[24] J. D. Holt, J. Menéndez, and A. Schwenk, Eur. Phys. J. **A49**, 39 (2013).
[25] J. D. Holt, J. Menéndez, and A. Schwenk, Phys. Rev. Lett. **110**, 022502 (2013).
[26] J. D. Holt, J. Menéndez, and A. Schwenk, J. Phys. G **40**, 075105 (2013).
[27] A. Gallant, J. Bale, T. Brunner, U. Chowdhury, S. Ettenauer, *et al.*, Phys. Rev. Lett. **109**, 032506 (2012).
[28] F. Wienholtz, D. Beck, K. Blaum, C. Borgmann, M. Breitenfeldt, *et al.*, Nature **498**, 346 (2013).
[29] M. Hjorth-Jensen, T. Kuo, and E. Osnes, Phys. Rept. **261**, 125 (1995).
[30] J. D. Holt, J. W. Holt, T. T. S. Kuo, G. E. Brown, and S. K. Bogner, Phys. Rev. C **72**, 041304 (2005).
[31] A. F. Lisetskiy, B. R. Barrett, M. K. G. Kruse, P. Navrátil, I. Stetcu, and J. P. Vary, Phys. Rev. C **78**, 044302 (2008).
[32] A. F. Lisetskiy, M. K. G. Kruse, B. R. Barrett, P. Navrátil, I. Stetcu, *et al.*, Phys. Rev. C **80**, 024315 (2009).
[33] K. Tsukiyama, S. K. Bogner, and A. Schwenk, Phys. Rev. Lett. **106**, 222502 (2011).
[34] K. Tsukiyama, S. K. Bogner, and A. Schwenk, Phys. Rev. C **85**, 061304(R) (2012).
[35] S. K. Bogner, R. J. Furnstahl, and R. J. Perry, Phys. Rev. C **75**, 061001(R) (2007).
[36] R. Roth, J. Langhammer, A. Calci, S. Binder, and P. Navrátil, Phys. Rev. Lett. **107**, 072501 (2011).
[37] D. R. Entem and R. Machleidt, Phys. Rev. C **68**, 041001 (2003).
[38] S. K. Bogner, R. J. Furnstahl, and A. Schwenk, Prog. Part. Nucl. Phys. **65**, 94 (2010).
[39] E. D. Jurgenson, P. Navrátil, and R. J. Furnstahl, Phys. Rev. Lett. **103**, 082501 (2009).
[40] P. Navrátil, Few-Body Systems **41**, 117 (2007).
[41] R. Roth, A. Calci, J. Langhammer, and S. Binder, (2013), arXiv:1311.3563 [nucl-th].
[42] H. Hergert and R. Roth, Phys. Lett. B **682**, 27 (2009).

[43] B. A. Brown and W. A. Richter, Phys. Rev. C **74**, 034315 (2006).
[44] A. Volya and V. Zelevinsky, Phys. Rev. Lett. **94**, 052501 (2005).
[45] C. Caesar *et al.* (R3B collaboration), Phys. Rev. C **88**, 034313 (2013).
[46] R. Kanungo, C. Nociforo, A. Prochazka, T. Aumann, D. Boutin, *et al.*, Phys. Rev. Lett. **102**, 152501 (2009).
[47] E. Lunderberg, P. DeYoung, Z. Kohley, H. Attanayake, T. Baumann, *et al.*, Phys. Rev. Lett. **108**, 142503 (2012).
[48] M. Stanoiu, F. Azaiez, Z. Dombradi, O. Sorlin, B. A. Brown, *et al.*, Phys. Rev. C **69**, 034312 (2004).
[49] B. Fernandez-Dominguez, J. Thomas, W. Catford, F. Delaunay, S. Brown, *et al.*, Phys. Rev. C **84**, 011301 (2011).
[50] Z. Elekes, Z. Dombradi, N. Aoi, S. Bishop, Z. Fulop, *et al.*, Phys. Rev. Lett. **98**, 102502 (2007).
[51] A. Schiller, N. Frank, T. Baumann, D. Bazin, B. A. Brown, *et al.*, Phys. Rev. Lett. **99**, 112501 (2007).
[52] C. Hoffman, T. Baumann, D. Bazin, J. Brown, G. Christian, *et al.*, Phys. Lett. **B672**, 17 (2009).
[53] K. Tshoo, Y. Satou, H. Bhang, S. Choi, T. Nakamura, *et al.*, Phys. Rev. Lett. **109**, 022501 (2012).